From Agri-Food Wastes to Polyhydroxyalkanoates through a Sustainable Process

Characteristics of polaritonic interactions at chiral loaded temperature-sensitive material (TSM) interfaces

OPEN ACCESS
IOP Publishing
Journal of Optics
J. Opt. **27** (2025) 025002 (15pp)
https://doi.org/10.1088/2040-8986/adabf7

Characteristics of polaritonic interactions at chiral loaded temperature-sensitive material (TSM) interfaces

Ahtisham Ali[1], **Muhammad Zeshan Yaqoob**[2,3,*], **Majeed A S Alkanhal**[4], **Abdul Ghaffar**[5] **and Yasin Khan**[4]

[1] Dipartimento di Elettronica e Telecomunicazioni, Politecnico di Torino, Torino, Italy
[2] Department of Physics, Government College University, 38000 Faisalabad, Pakistan
[3] Higher Education Department (HED), Government of Punjab, Lahore, Pakistan
[4] Department of Electrical Engineering, King Saud University, Riyadh, Saudi Arabia
[5] Department of Physics, University of Agriculture, Faisalabad, Pakistan

E-mail: zeeshaan32@yahoo.com

Received 23 October 2024, revised 10 January 2025
Accepted for publication 20 January 2025
Published 29 January 2025

Abstract

Polaritonic interactions are pivotal in advancing sensing technologies, optical devices, and waveguides. This study presents a theoretical investigation into polaritonic interactions at the interface of chiral-loaded temperature-sensitive materials (TSMs). Indium antimonide (InSb), known for its temperature-dependent phase-transition optical properties, is utilized as the TSM. The electromagnetic (EM) behavior of InSb is described using the extended Drude model, while the isotropic chiral medium is characterized through coupled constitutive relations. By applying tangential boundary conditions for EM field continuity at the chiral–InSb interface, the dispersion relation governing hybrid polaritons is derived. Numerical computations performed in Wolfram Mathematica, utilizing the contour plot technique, reveal the dispersion characteristics, effective mode index, and field distributions under varying temperatures. The findings demonstrate the existence of two distinct polaritonic regimes: (i) hybrid polariton–phonon coupling at temperatures below 200 K, and (ii) hybrid polariton–plasmon coupling at temperatures exceeding 260 K. Additionally, the effects of chirality and temperature on the dispersion curves, effective mode indices, and field profiles are systematically analyzed. Results reveal that polaritonic surface modes can be dynamically tuned by manipulating external temperature and material chirality. These insights hold significant promise for the development of temperature-responsive terahertz-infrared sensors, enantiomeric detectors, thermo-optical surface waveguides, and near-field imaging systems.

Keywords: polaritons, plasmons, phonons, terahertz, infrared, thermo-optical, indium anstimonide

* Author to whom any correspondence should be addressed.

1. Introduction

Polaritonic interactions have garnered significant interest from many researchers because of their crucial role in sensing, communication, and optoelectronic devices [1]. Polaritons are quasi-particles that emerge as a consequence of strong light–matter interactions [2]. Polaritons are sensitive to material types and light frequencies. Depending upon the features of materials and interacting light, polaritons can be classified into various types (i.e. phonon-polaritons, plasmon-polaritons, magnon-polaritons, and exciton-polaritons) [3]. Generally, the excitation of plasmon-polaritons, phonon-polaritons, exciton-polaritons, and magnon-polaritons requires metallic materials, dielectric crystals, semiconductor materials, and magnetic materials, respectively [4]. Recent technological innovations in device fabrication techniques, controlled material growth, imaging, and spectroscopic techniques have enabled researchers to realize a wide range of polaritonic resonances, which can be used to control coherence, nonlinearity, and light–matter interactions [5].

In the literature, polaritonic interactions have been studied via two approaches (i.e. cavity-based optical systems and surface optics) [6, 7]. In cavity-based optical systems, the confined photons interact with the materials inside to excite the polaritonic resonances within the mirrors [8], while in the surface optics approach, the free photons interact with the surface materials/coatings/geometry-based oscillations to evolve the polaritonic interactions [9]. Santos and Fainstein recently introduced a new field of physics, polaromechanics, combining cavity polaritons and optomechanics, and discussed its challenges and opportunities [10]. The different types of polaritonic interactions have been studied via optical cavities based upon different materials. For example, Harrison *et al* the oretically investigated the existence of polariton vortices supported by the Chern insulator and proposed optical-based topological signal processing techniques [11]. Baranov *et al* conducted transfer-matrix-based analytical and finite-difference time-domain simulations of the enhancement of the polaritonic modes within the resonant optical cavity due to chiral molecules and reported that the circular dichroism (CD) of the chiral material introduces the splitting of the polaritonic and plasmonic modes of the microcavity [12]. Bennenhei *et al* analyzed the thermal polaritonic interactions of protein-filled elliptical microcavities under controlled polarization schemes at room temperature and observed photoluminescence-based exciton-polaritons emerging from elliptical microcavities [13]. Further, Król *et al* discussed microcavity-based general schemes for the excitation of polaritonic modes in WS2 monolayers, spin-coated PEPI perovskites, and CdTe quantum wells [14]. Recently, Salij et.al theoretically investigated the rare opportunity of developing 2D chiral polaritons due to achiral Fabry-Pérot cavities and reported that apparent CD can excite 2D chiral polaritons and their chirality can be optimized for the advancement of lasing applications, sensing, and quantum computing [15].

Meanwhile, on the other side, the surface optics domain provides the active control and tuning of polaritonic interactions in terms of electromagnetic (EM) surface modes for the different spectral ranges (i.e. metastructures, nanostructures, and zero indexed materials) [16–18]. Many plasmonic platforms for the visible range have been investigated for their strong interactions with nanostructures and biomolecules, offering potential applications in waveguides, biosensing, drug delivery, and nanophotonics [19–21]. Generally, the dichroism phenomenon has been observed in organic, inorganic, and biological molecules. This phenomenon can be controlled by the strength of the chirality, which normally ranges from 10^{-2} to 10^{-7}, depending on the type and structure of the molecules [22, 23]. These molecules are regarded as chiral materials and have attracted the interest of several researchers and scientific communities as tools for enantiomer detection, chemical or analyte sensing, and chiral sensing [24]. In order to generate hybrid SPP waves for chiral sensing and enantiomeric detection, researchers have recently focused on the chiral–metal interface. It has also been reported that the propagation length can be used to tune chirality [25]. Many researchers have recently developed a keen interest in graphene-based temperature-assisted devices due to their uses in thermographers, wearable temperature sensors, thermal current production, thermal rectifiers, and infrared (IR) detectors [26–28]. Hybrid SPP waves along the chiral–graphene–metal interface whose properties can be tuned for various applications, including wave modulation and optical sensing in the terahertz (THz) region, have been reported [29]. Recently, it has been reported that the characteristics of surface waves supported by graphene loaded InSb can be controlled by tuning the temperature [30]. Similarly, it has been hypothesized that a chiral–temperature-sensitive material (TSM) structure may be used to control the characteristics of such surfaces as plasmon-polaritons, and this has motivated the present work.

Indium antimonide (InSb) is a TSM known for its semiconductor-like properties. The optical, electronic, structural, and phase characteristics of TSMs can be tuned by changing the external temperature [31]. InSb has recently gained interest as a promising material for IR detectors and high-speed devices due to its small bandgap [32].

InSb is recognized for its temperature-dependent phase-changing optical properties, making it a key TSM. This work investigates the temperature-dependent polaritonic interactions governed by the chiral loaded InSb interface. To study the influence of thermal agitation, polaritonic interactions and coupling schemes are investigated. Further, to investigate the impact of the dichroism of the chiral material on the right-handed circularly polarized (RCP) and left-handed circularly polarized (LCP) field coupling, enhancement parameters are investigated. The thermal tuning of chiral surface modes is the most challenging task and is needed for the realization of real-time chiral recognition, enantiomeric measuring, and chiral sensing devices. To fulfil this need, the chiral loaded InSb is modeled and analyzed numerically for the active tuning and control of such hybrid surface waves in the IR and

THz region. This paper investigates wave propagation along the chiral–TSM interface. The effects of chirality (ξ) and temperature on the dispersion curves, effective mode index, and field profiles of hybrid surface waves are studied for the lower and the upper propagation modes. The analytical modeling and formulation of the problem are presented in the second section, while the numerical results and discussion are detailed in the third section. Concluding remarks are provided in the fourth section.

2. Modeling of problem

The present polaritonic waveguide system comprised of the temperature-sensitive InSb substrate loaded with the chiral material is shown in figure 1. The propagation of the surface polaritonic modes is considered along the z-axis with propagation constant β. The region of space $x > 0$ is realized as isotropic chiral material and the region $x < 0$ is taken as a TSM with temperature-dependent permittivity $\in_T(\omega, T)$ [33].

2.1. Field phasors in isotropic chiral material

The isotropic chiral material is modeled in the frame work of coupled constitutive relations as [34, 35],

$$\left.\begin{aligned} \boldsymbol{D} &= \varepsilon\, \boldsymbol{E} - i\xi \boldsymbol{B} \\ \boldsymbol{H} &= -i\,\xi\, \boldsymbol{E} + \boldsymbol{B}/\mu \end{aligned}\right\} \tag{1}$$

where the ε is permittivity, μ is the permeability and ξ is the chirality of the chiral material. The generalized expression for the EM wave in the chiral material is

$$\nabla^2 E - \mu\,\varepsilon\,\frac{\partial^2 E}{\partial t^2} + i\,\xi\,\mu\frac{\partial}{\partial t}(\nabla \times E) = 0\,. \tag{2}$$

For the planar interface, it is assumed that electric (E) and magnetic (H) fields are functions of spatial coordinates (x, y, z). The EM wave is considered to propagate along the z-axis while exhibiting an exponential decay along the x-axis. The field phasors represented as a superposition of right-handed circularly polarized (RCP) and left-handed circularly polarized (LCP) modes (ψ_1 & ψ_2) are expressed as:

$$E_z = [\psi_1 + \psi_2]\, e^{-j\beta z} \tag{3}$$

$$H_z = j\eta_c\sqrt{1+\chi^2}\,[\psi_1 - \psi_2]\, e^{-j\beta z} \tag{4}$$

where the modes $\psi_1 = B_1 e^{-\gamma_1 x}$, $\psi_2 = B_2 e^{-\gamma_2 x}$, and decay constants are $\gamma_{1,2} = \sqrt{\beta^2 - \gamma_\pm^2}$. The B_1 and B_2 are considered as unknown coefficients associated with RCP and LCP modes respectively. The propagation constants for RCP and LCP are expressed as $\gamma_\pm = n_c(\pm\chi + \sqrt{1+\chi^2})k_o$, in this expression k_o is wavenumber in free space, $k_o = \omega\sqrt{\mu_o \in_o}$, n_c is the refractive index of chiral material and $\chi = \xi/\eta_c$ is the normalized chirality admittance.

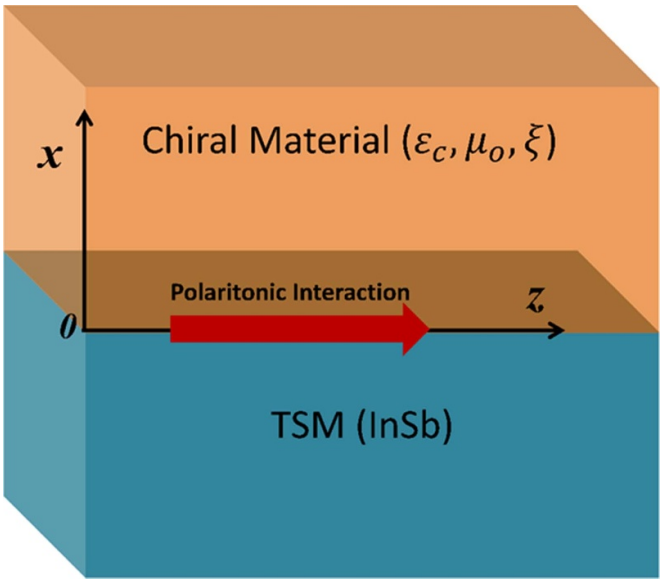

Figure 1. Isotropic chiral loaded TSM structure for polaritonic interaction.

The associated field components within the chiral medium can be derived from the coupled wave equation as follows:

$$E_x = -\left[\left(\frac{j\beta}{\gamma_1}\right)B_1 e^{-\gamma_1 x} + \left(\frac{j\beta}{\gamma_2}\right)B_2 e^{-\gamma_2 x}\right] e^{-j\beta z} \tag{5}$$

$$H_x = \eta_c\sqrt{1+\chi^2}\left[\left(\frac{\beta}{\gamma_1}\right)B_1 e^{-\gamma_1 x} - \left(\frac{\beta}{\gamma_2}\right)B_2 e^{-\gamma_2 x}\right] e^{-j\beta z} \tag{6}$$

$$E_y = -\left[\left(\frac{\gamma_+}{\gamma_1}\right)B_1 e^{-\gamma_1 x} + \left(\frac{\gamma_-}{\gamma_2}\right)B_2 e^{-\gamma_2 x}\right] e^{-j\beta z} \tag{7}$$

$$H_y = -\eta_c\sqrt{1+\chi^2}\left[\left(\frac{\gamma_+}{\gamma_1}\right)B_1 e^{-\gamma_1 x} - \left(\frac{\gamma_-}{\gamma_2}\right)B_2 e^{-\gamma_2 x}\right] e^{-j\beta z}. \tag{8}$$

2.2. Field phasors in TSM

The field phasors for the TSM space region ($x < 0$) are given as:

$$E_z = \mathrm{C}_1 e^{k_T x} \tag{9}$$

$$H_z = \mathrm{C}_2 e^{k_T x} \tag{10}$$

$$E_x = \frac{j\beta}{k_T}\,E_z \tag{11}$$

$$H_x = \frac{j\beta}{k_T}\,H_z \tag{12}$$

$$E_y = -\frac{j\omega\mu_o\beta}{k_T}H_z \tag{13}$$

$$H_y = -\frac{j\omega\in_T\beta}{k_T}E_z, \tag{14}$$

where $k_T = \sqrt{\beta^2 - \omega^2\mu_o\in_T}$ is the decaying constant, C_1 and C_2 are supposed as unknown field coefficients. The $\in_T$ is the

relative permittivity of InSb and is expressed according to the extended Drude model and can be tuned by varying the temperature, the detail of the model has been provided in subsequent section.

The characteristic equation for surface polaritonic excitations at the chiral–TSM interface ($x = 0$) can be computed by securing the continuity of the fields governed by the boundary conditions [29]

$$\left.\begin{aligned} \boldsymbol{u_x} \times (\boldsymbol{E_C} - \boldsymbol{E_T}) = 0 \\ \boldsymbol{u_x} \times (\boldsymbol{H_C} - \boldsymbol{H_T}) = 0 \end{aligned}\right\} \tag{15}$$

expressed as

$$\begin{aligned} &\left(\omega\mu_o\eta_c\sqrt{1+\chi^2}\gamma_1 + \gamma_+ k_T\right)\left(\frac{\omega\in_T}{\eta_c\sqrt{1+\chi^2}}\gamma_2 + \gamma_- k_T\right) \\ &+ \left(\omega\mu_o\eta_c\sqrt{1+\chi^2}\gamma_2 + \gamma_- k_T\right)\left(\frac{\omega\in_T}{\eta_c\sqrt{1+\chi^2}}\gamma_1 + \gamma_+ k_T\right) = 0, \end{aligned} \tag{16}$$

where the terms ($\boldsymbol{E_c}$, $\boldsymbol{H_c}$) and ($\boldsymbol{E_T}$ & $\boldsymbol{H_T}$) in the boundary conditions are the total EM fields in the chiral and TSM materials. The first and third terms in the above expression represent dispersion relations for the TE waves, whereas the second and fourth terms represent dispersion relations for the transverse magnetic (TM) waves. At $\gamma_+ = \gamma_-$, the above relation simplifies to the same dispersion relation for SPPs at the metal–dielectric interface, which supports only TM mode [36].

3. Numerical results and discussion

The characteristics of polaritonic interactions at the interface of chiral loaded TSM InSb, including dispersion relations, effective mode index, and field profiles, were obtained numerically using the contour plot technique. The Wolfram Mathematica software Pack was used for the numerical simulation of each characteristic of the surface waves. In the first part, the modeling of the InSb based upon the extended Drude model [33, 37] as a function of the static permittivity ($\in_\infty$), plasma frequency (ω_p), and damping constant (γ) has been presented as

$$\in_T = \in_\infty - \frac{\omega_p^2}{\omega^2 + i\gamma\omega} \tag{17}$$

ω_p is expressed as $\omega_p = \sqrt{\frac{Nq_e}{0.015\,\varepsilon_o m_e}}$, where N is the intrinsic carrier density, m_e is the mass of an electron, and q_e is the charge on an electron (i.e. $q_e = -1.6 \times 10^{-19}$ C, $m_e = 9.1 \times 10^{-31}$ kg, $\gamma = \pi \times 10^{11}$ rad s^{-1}). Mathematically, the intrinsic carrier density $N(T)$ is expressed as a function of external temperature as $N(T) = 5.76 \times 10^{20}\, T^{3/2} \exp\left(-\frac{E_g}{2k_B T}\right)$, while E_g and k_B correspond to the energy bandgap and Boltzmann constant with values of 0.26 eV and 8.62×10^{-5} eV K^{-1}, respectively. The intrinsic carrier density $''N''$ depends upon the temperature $'T'$ which implies that the plasma frequency is driven by the temperature of InSb. Consequently, the relative permittivity of InSb ($\in_T$) can be tuned by varying the temperature. The influences of the temperature of InSb and the chirality of the chiral material on the characteristics of polaritonic interactions at the interface of chiral InSb were explored.

In figure 2, we plot the graph of the plasma oscillation (ω_p) of the InSb slab for the temperature range $T \in [150 - 200]$ K (insulator case) and $T \in [260 - 400]$ K (metallic case). It shows that the polaritonic interactions increase significantly with the temperature of InSb. Thus, the permittivity of InSb can be tuned by changing the temperature according to the desired spectral region [37].

Given the active thermal tunability of InSb, the external temperature plays a significant role in tuning the light–matter interaction characteristics. To study the temperature-dependent surface polaritonic interactions for InSb, a dispersion curve analysis was conducted. The results of the comparative dispersion curve analysis for bare InSb and chiral loaded InSb are presented in figures 3 and 4, respectively. In figures 3(a) and (b), the dispersion relation for bare InSb is plotted for the insulator and metallic states for the temperatures 190 K and 300 K, respectively. The coupling between plasmons and phonons, which gives rise to polaritonic interactions, is evident from the graph. Figure 3(a) depicts the phono-polariton coupling at the interface of bare InSb under the insulator phase, while figure 3(b) presents the plasmon-polariton coupling under the metallic phase of InSb. It can be concluded that the excitation of phononic resonance at low THz frequency is due to the insulator phase of InSb, while the plasmonic resonance at high THz frequency corresponds to the metallic phase of InSb. This trend is visualized in figure 2, where ω_p corresponds to low THz frequency for $T \in [150 - 200]$ K (insulator state) of InSb, while for $T \in [260 - 400]$ K (metallic state) of InSb, it corresponds to high THz frequency, as reported in [38].

After estimating the phononic and plasmonic interactions at the interface of bare InSb, the dispersion curve analysis for the chiral loaded InSb interface is discussed. Figure 4 depicts the influence of CD or chirality (ξ) on the light coupling phenomenon on the surface of InSb. It is observed that the presence of chirality (ξ) initiates hybridization-based splitting among the polaritonic interactions (i.e. hybrid phonon-polariton modes for $T = 190$K and hybrid plasmon-polariton modes for $T = 300$K). Figures 4(a) and (b) reveals that there exist two propagation modes for this geometry (i.e. the lower and upper modes for the low and high frequencies, respectively, collectively known as hybrid modes). Similar splitting in plasmonic modes has been reported with the cavity-based chiral optical system, which validates the present findings [12].

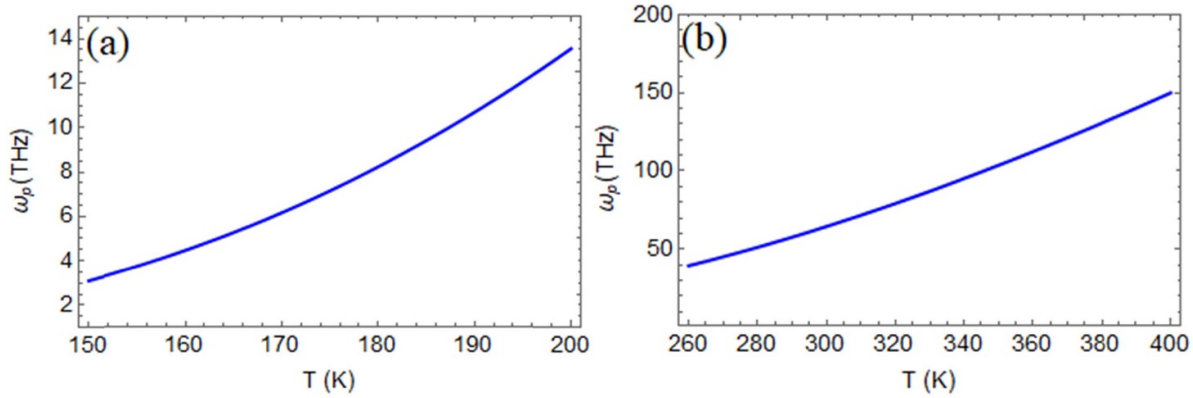

Figure 2. Modeling of InSb as temperature sensitive material (TSM) (a) insulator case (b) metallic case.

The dispersion curves for the polaritonic interactions at the chiral loaded InSb at different temperatures (i.e. $T = 280$ K, $T = 300$ K, $T = 320$ K, and $T = 340$ K) are plotted in figure 5. Figure 5(a) depicts that high-frequency surface waves and propagation modes (lower and upper) can be achieved with the increase in temperature even in the dielectric case of TSM ($T = 160$ K, $T = 180$ K, and $T = 200$ K). It is also clear from figure 5(b) that with the temperature rise, the behavior of the TSM (i.e. InSb) moves toward metallic from dielectric, and surface waves of high frequency with both modes (lower and upper) can be achieved and tuned. The effect of chirality on the dispersion curves for chiral loaded InSb at different temperature values is plotted in figure 6. The graph shows a clear increase in the polaritonic interactions at the interface and propagation bandgap between the modes with an increase in the chirality in both the dielectric ($T = 190$ K) and metallic ($T = 300$ K) cases. As depicted in figures 6(a) and (b), the forbidden region between both modes gradually narrows as chirality increases. Thus, chirality, acting as a controlling parameter, can be effectively used to tune the propagation of hybrid surface waves.

To evaluate the propagation losses and attenuation characteristics of polaritonic interactions at the chiral–TSM interface, the relationship between the operating frequency (ω) and the imaginary part of the propagation constant, Im(β), is analyzed in figures 7 and 8 under the influence of temperature and chirality, respectively. The magnitude of Im(β) serves as a measure of attenuation and propagation losses of EM waves, with higher Im(β) values indicating greater damping [39].

In figure 7, the impact of temperature on the propagation loss of polaritonic modes is analyzed. Figure 7(a) illustrates the damping and propagation losses of polariton modes when InSb behaves as an insulator, while figure 7(b) presents the propagation losses at the chiral–TSM interface under metallic conditions. It is observed that as the temperature increases, the propagation loss rises with the operating frequency up to the resonance frequency for each case. As discussed in figure 2, the plasma frequency of InSb is directly influenced by temperature. Consequently, in this scenario, the propagation losses stabilize at the resonance frequency and decrease to minimal values for frequencies exceeding the resonance condition.

To investigate the influence of chirality on the damping characteristics of the chiral–TSM interface, results are presented in figures 8(a) and (b) for $T = 190$ K (insulator case) and $T = 300$ K (metallic case), respectively. A comparison of these figures reveals that the propagation losses are lower in the insulator case than in the metallic case. However, the frequency-dependent behavior of Im(β) follows a similar trend in both cases. Notably, the propagation loss increases with rising chirality in both scenarios. Additionally, it can be concluded that chirality does not influence the damping response at the resonance frequency of InSb. Furthermore, Mackay and Lakhtakia have theoretically investigated the simultaneous amplification and attenuation of surface waves in isotropic chiral materials [40]. Their findings indicate that the attenuation of surface waves at high chirality can be effectively managed and reduced by incorporating active material-based mixing into the chiral medium. Similarly, adopting such approaches could enhance propagation characteristics and minimize surface wave attenuation, offering practical avenues for the implementation of the present work.

The figure 9 provides the physical insight how the chiral sensing response against the effective mode index of polaritonic modes under different values of the temperature. The graph clearly shows that the chiral strength increases as the temperature increases for both cases of InSb. The results indicate the chiral strength enhancement as the $Re[\beta]/k_o$ increases for respective temperature. Meanwhile, the temperature has the significant impact on the chiral strength against the effective mode of polaritonic modes depicts that the thermal agitation can control the CD response of the material. Thus, the temperature can be used as a controlling parameter to tune the characteristics of hybrid surface waves by varying the chirality strength of chiral materials.

To further confirm the physical presence of hybrid surface modes corresponding to the upper and lower modes supported by the loaded InSb at $T = 190$ K, the field distribution is plotted in figures 10(a)–(d). All the fields are normalized

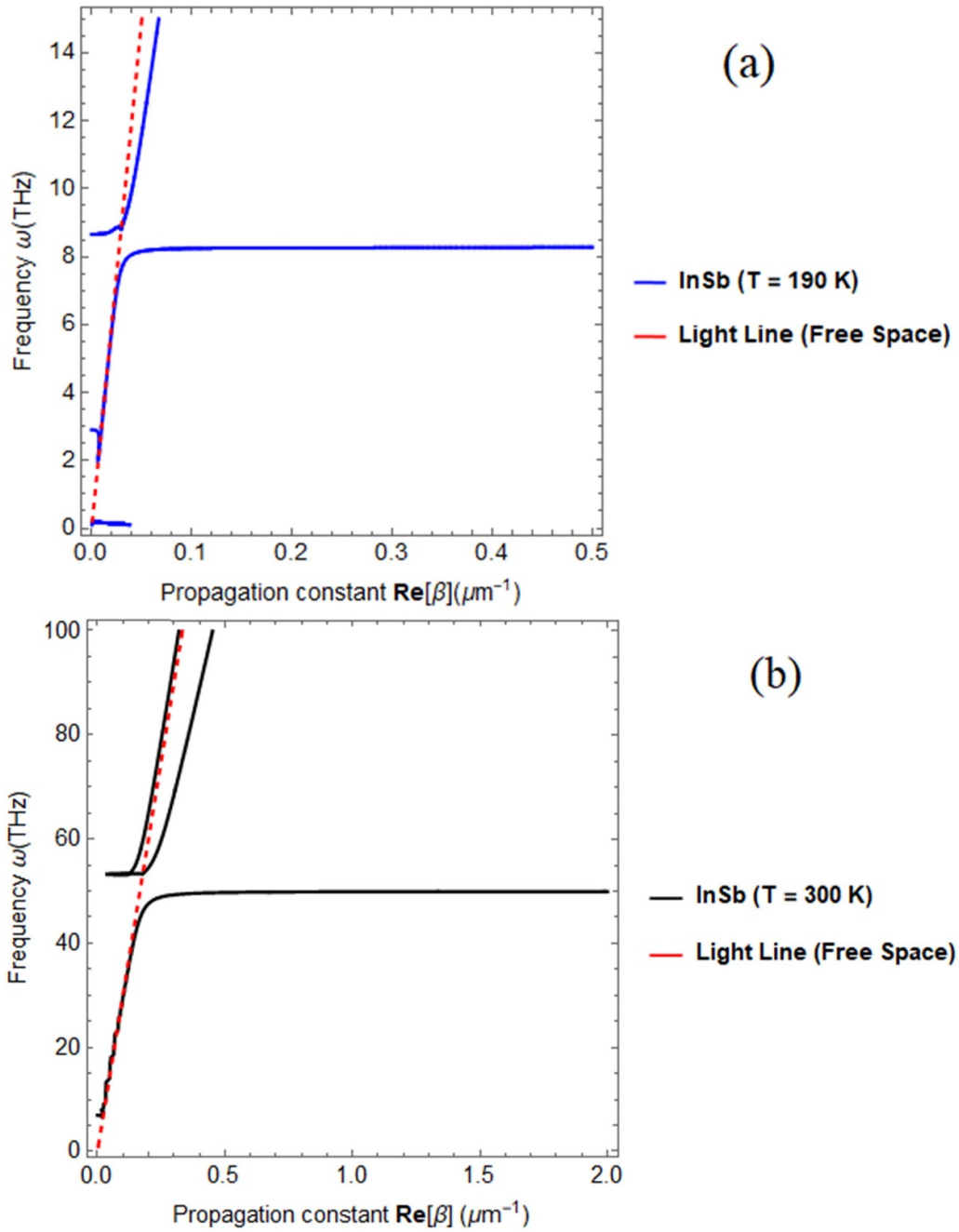

Figure 3. Dispersion curve for free space–InSb interface with $\xi = 0.0\Omega^{-1}$ (a) InSb as Insulator (T = 190 *K*) (b) InSb as metal ($T = 300$K).

by the peak value. The $|E_x|$ & $|E_y|$ fields components correspond to the TM and transverse electric (TE) components. The presence of both transverse field components in figures 10(c) and (d) indicates that the modes supported at the chiral–InSb interface are hybrid in nature. The figures 10(b) and (d) for the upper modes, illustrate that they decay exponentially as they propagate away from the interface, which confirms the surface polariton like nature of the modes. Moreover, it can be seen that the lower modes do not decay exponentially as the upper modes do. This could be because these modes do not correspond to the surface modes but to the chiral phononic polaritons with distinct co- and cross-polarized fields, as given in figure 10(3). The upper mode is more tightly confined to the interface, as evidenced by the rapid exponential decay of all field components in subplots 10(b) and (d). The lower mode shows weaker confinement, with fields extending farther into the chiral medium, as seen in subplots 10(a) and (c). Similarly, the field distribution for the lower and upper modes supported

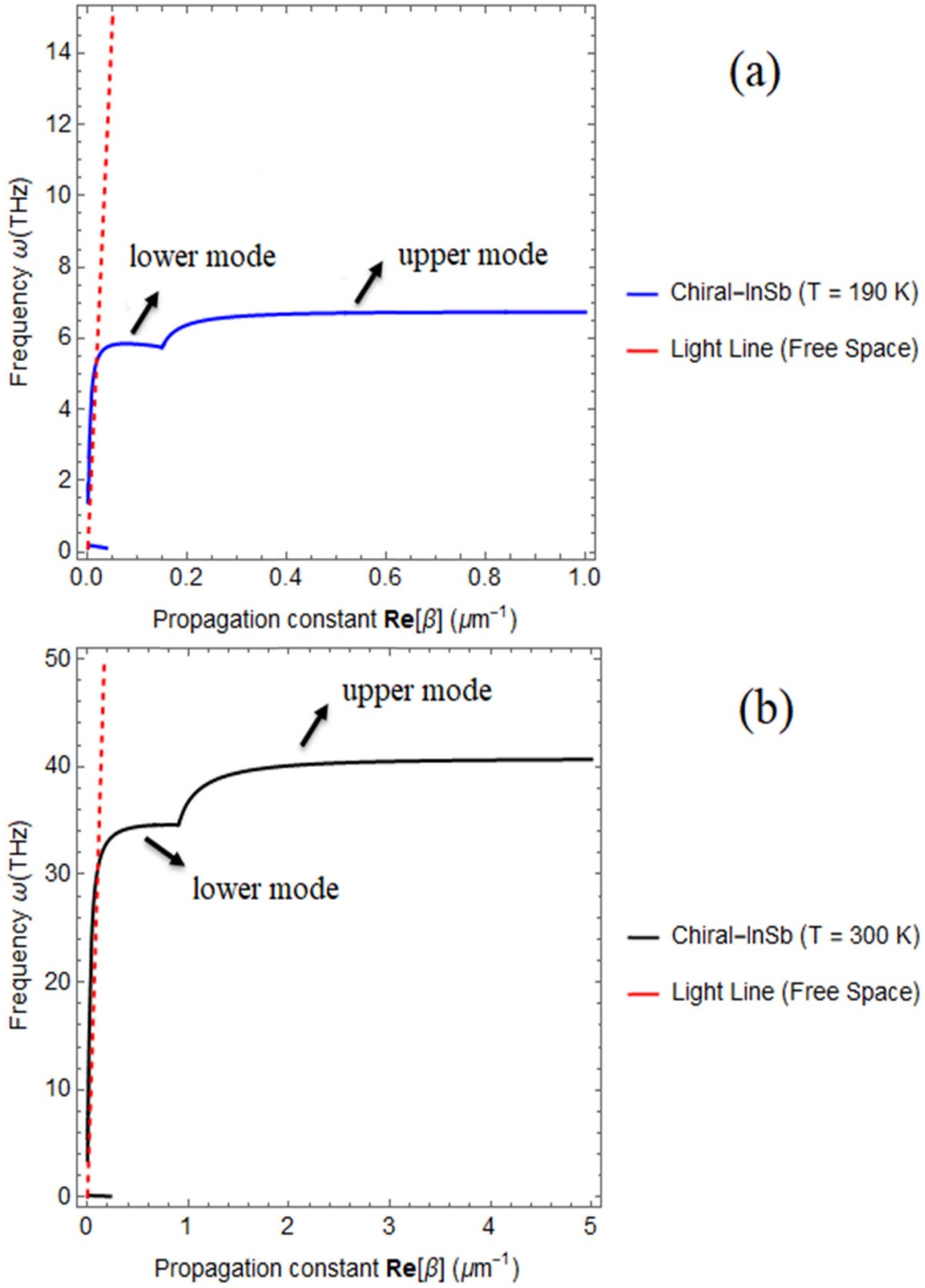

Figure 4. Dispersion curve for free space–InSb interface with $\xi = 0.01\Omega^{-1}$ (a) InSb as Insulator (T = 190 *K*) (b) InSb as metal ($T = 300$K).

at the chiral–InSb interface at $T = 300$ K is plotted graphically in figure 11. It is shown that the upper modes correspond to the surface-like modes and behave as hybrid surface plasmon-polaritons, while the lower modes correspond to the chiral plasmon-polariton propagation modes. However, figures 11(b) and (d) suggest that hybrid surface plasmon-polaritons decay more quickly than hybrid surface phonon-polaritons, as given in figures 10(b) and (d).

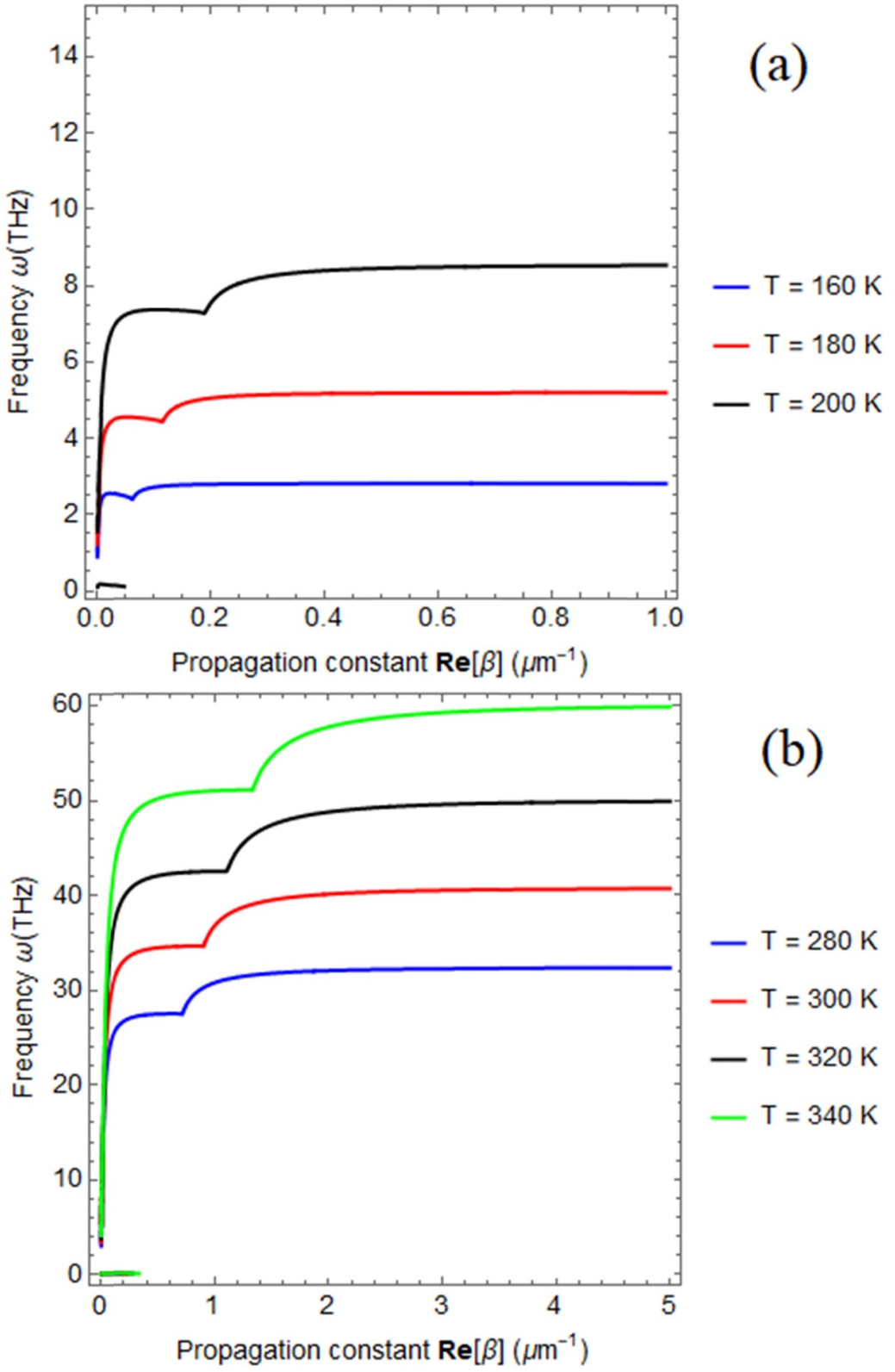

Figure 5. Dispersion curves for a chiral–InSb interface under varying temperatures with $\xi = 0.01\Omega^{-1}$ (a) InSb as insulator for $T \in [160,\ 180,\ 200]\,K$ (b) InSb as metal for $T \in [280,\ 300,\ 320,\ 340]\,K$.

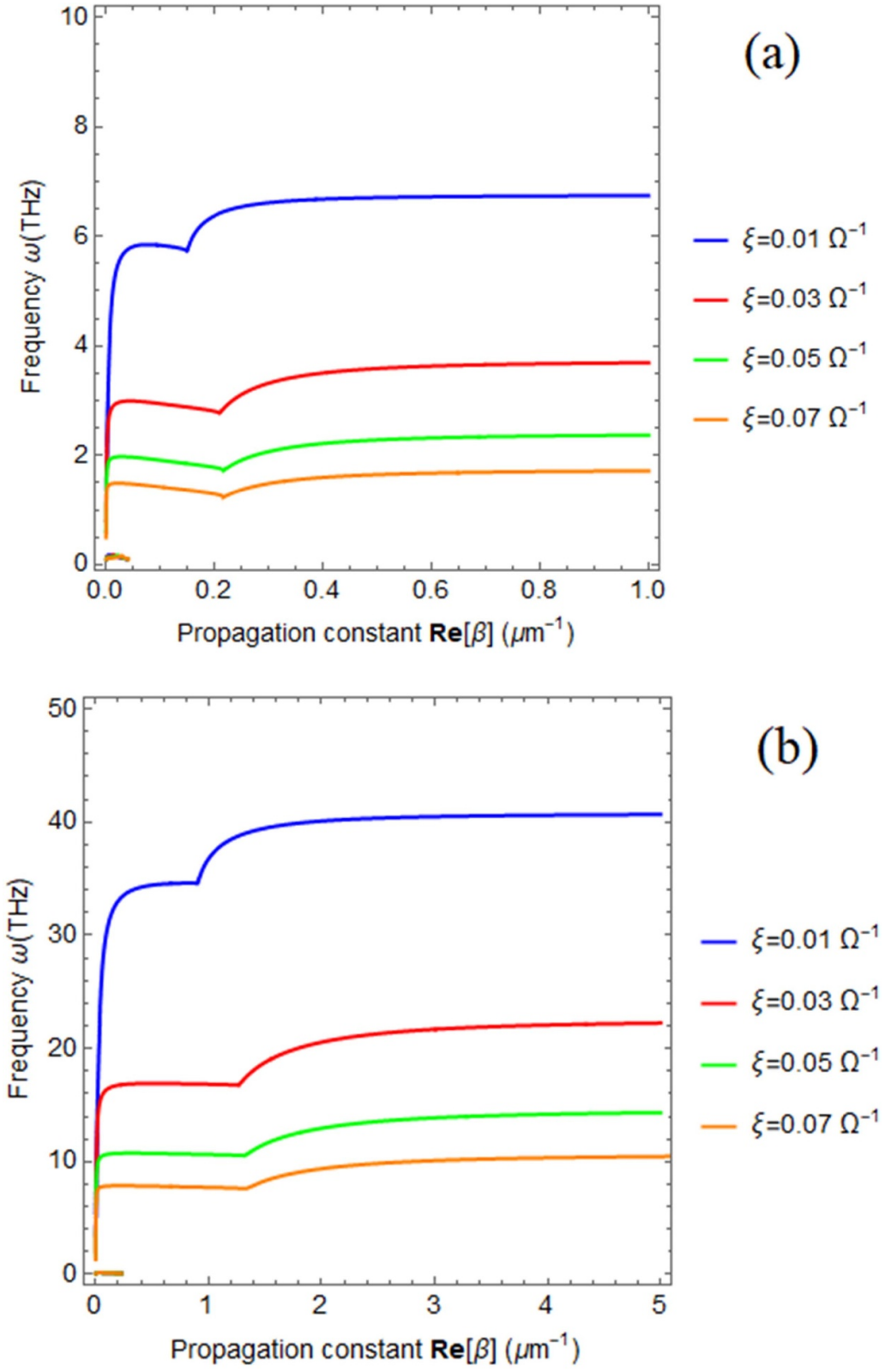

Figure 6. Dispersion curve for chiral–InSb interface under varying chirality (a) InSb as Insulator (T = 190 *K*) (b) InSb as metal (*T* = 300 K).

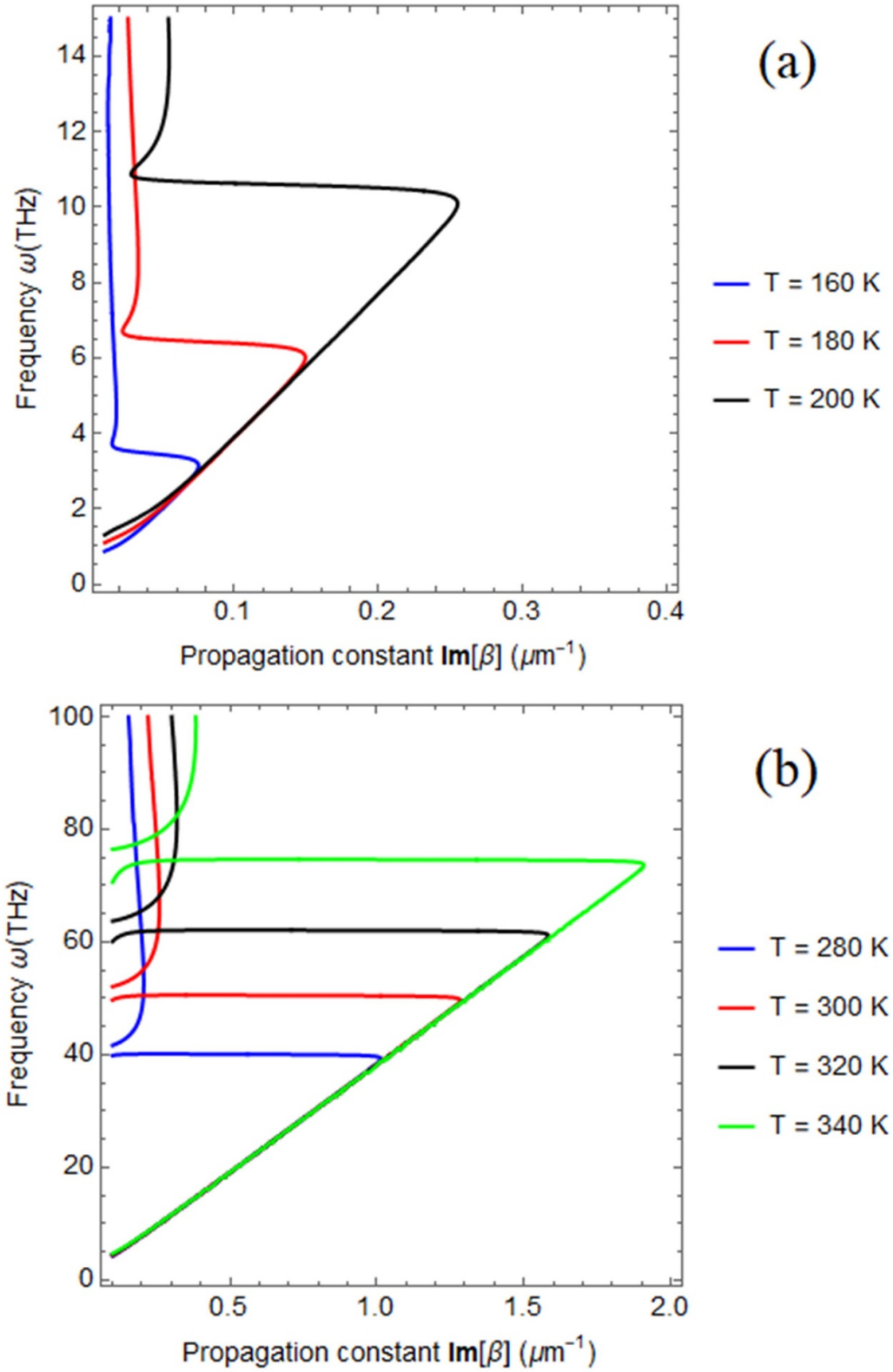

Figure 7. Propagation loss for chiral–InSb interface under varying temperature with $\xi = 0.01\Omega^{-1}$ (a) InSb as insulator for $T \in [160,\ 180,\ 200]\,K$ (b) InSb as metal for $T \in [280,\ 300,\ 320,\ 340]\,K$.

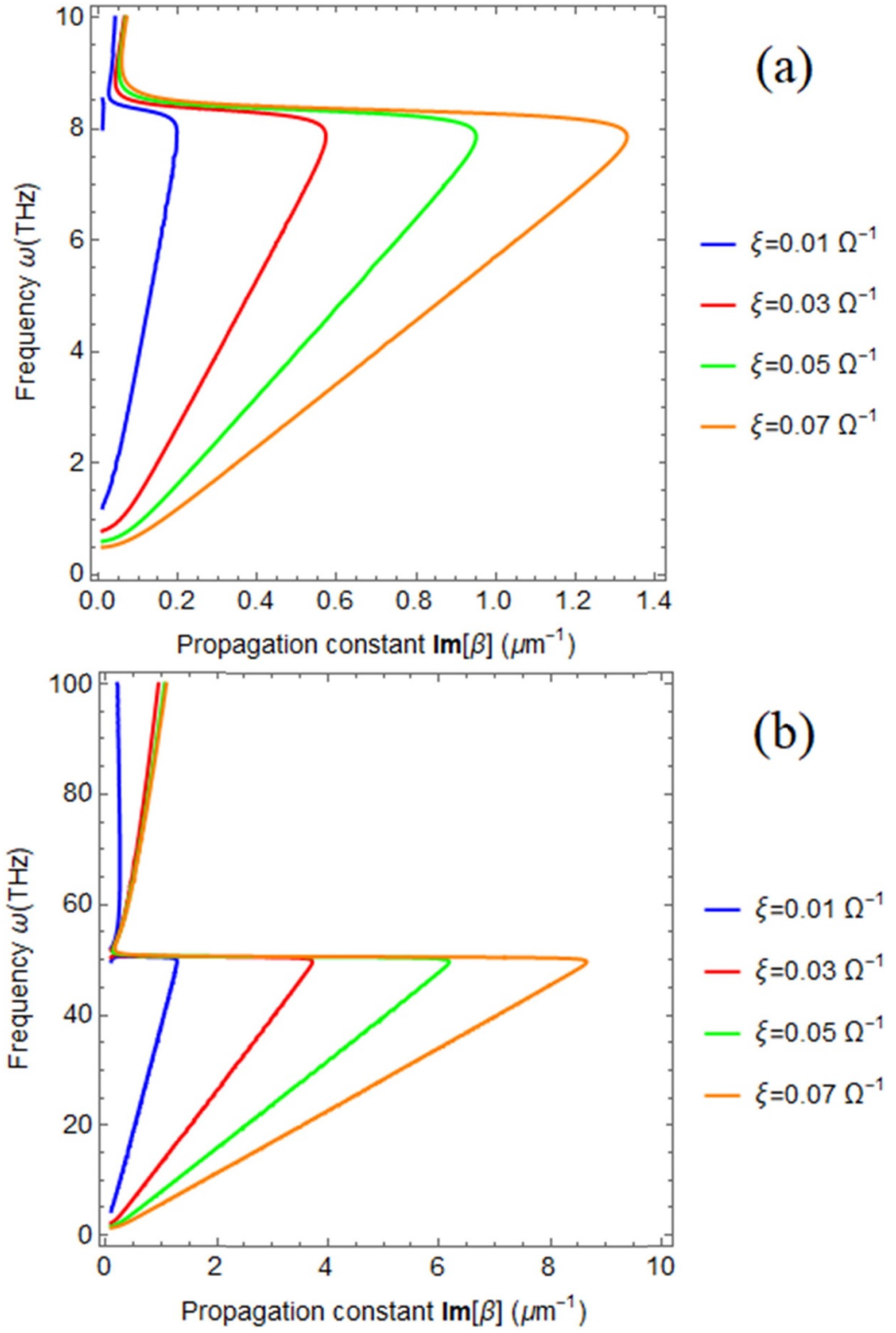

Figure 8. Propagation loss for chiral–InSb interface under varying chirality (a) InSb as Insulator (T = 190 *K*) (b) InSb as metal (*T* = 300 K).

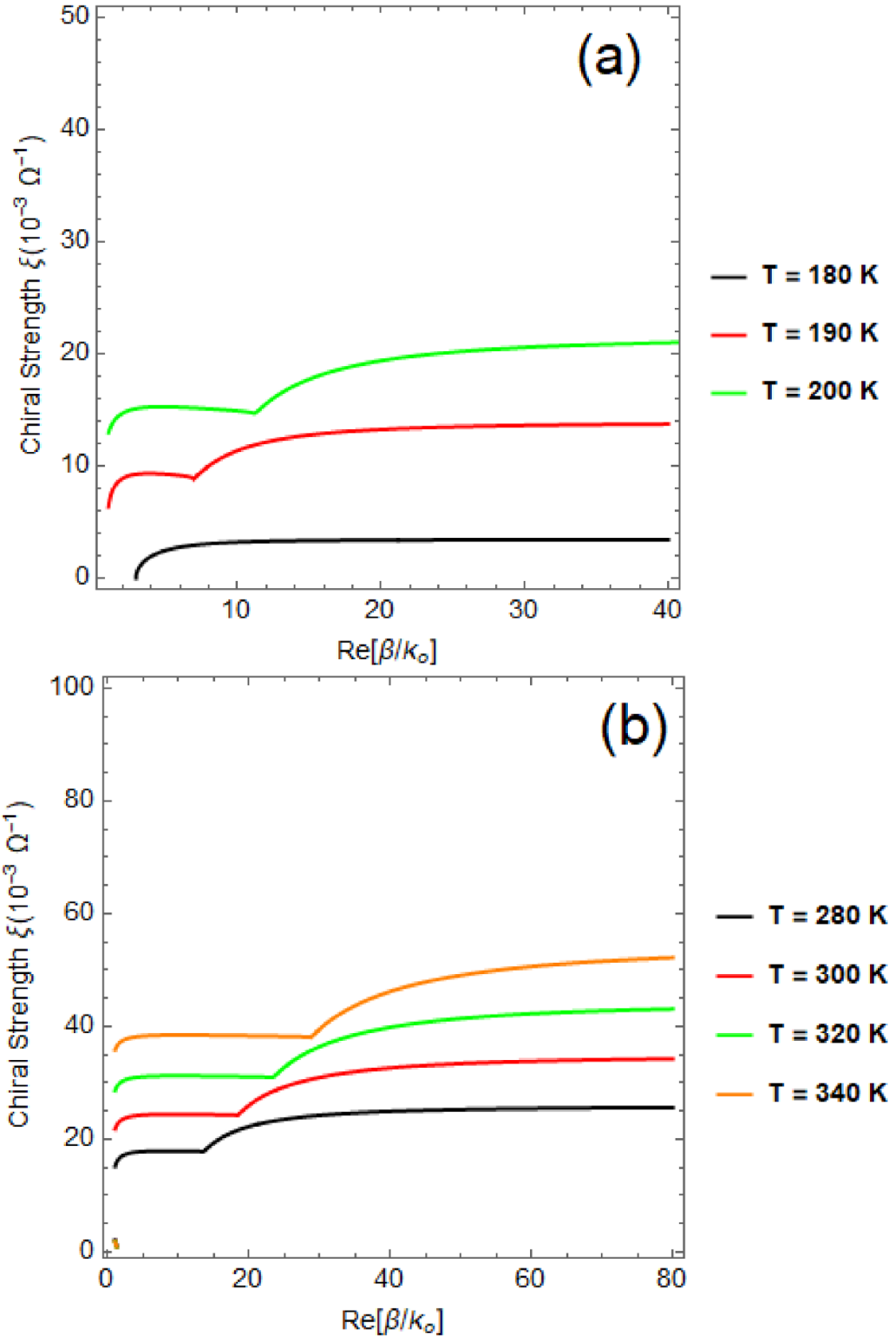

Figure 9. Chiral strength as function of confinement for chiral–InSb interface with $\omega = 6$ THz & $\varepsilon_c = 2.25\ \varepsilon_o$ (a) InSb as insulator for $T \in [180,\ 190,\ 200]\,K$ (b) InSb as metal for $T \in [280,\ 300,\ 320,\ 340]\,K$.

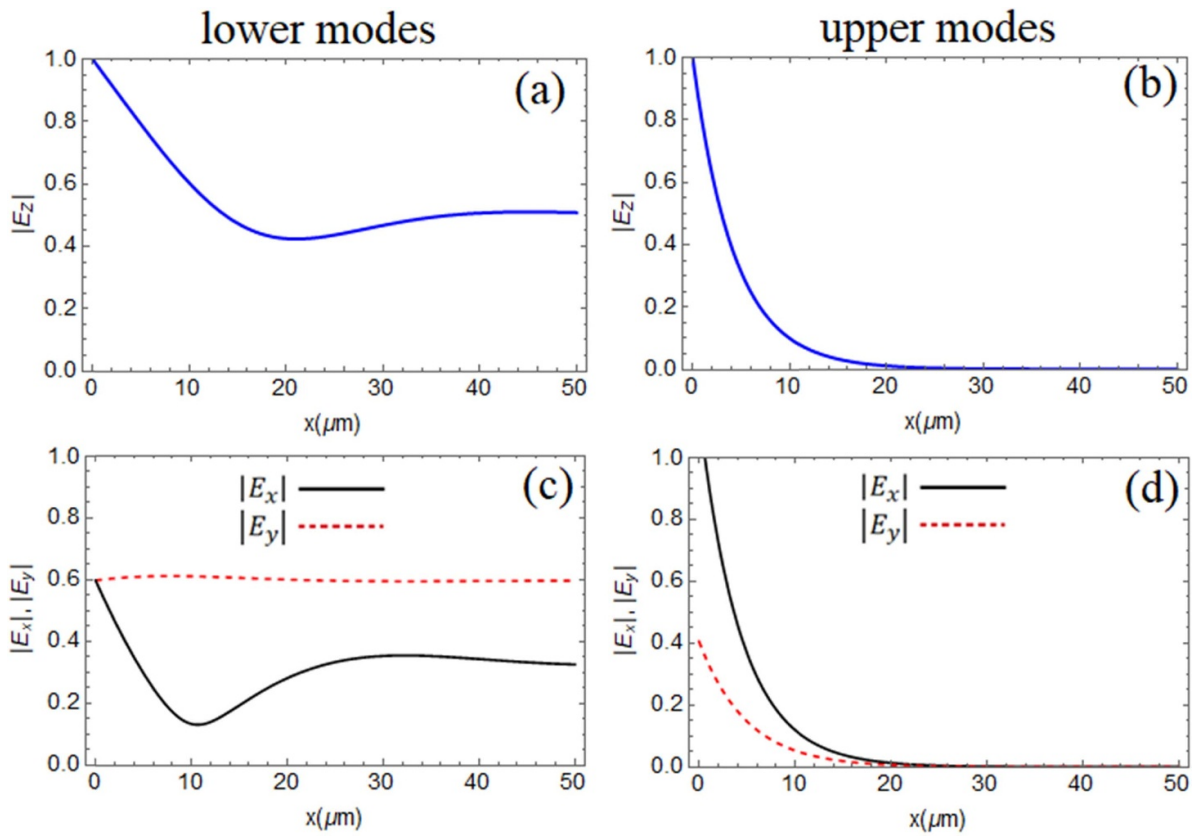

Figure 10. Field distribution as function of transverse distance at chiral–InSb interface for $T = 190$ K (insulator state), with $\xi = 0.01\Omega^{-1}$ & $\varepsilon_c = 2.25\ \varepsilon_o$ (a) Field profile of $|E_z|$ for lower mode with values $\beta = 0.0825\ \mu\text{m}^{-1}$, $\omega = 5.791$ THz; (b) Field profile of $|E_z|$ for upper mode with values $\beta = 0.266\ \mu\text{m}^{-1}$, $\omega = 6.537$ THz (c) Field profile of $|E_x|$, $|E_y|$ for lower mode with values $\beta = 0.0825\ \mu\text{m}^{-1}$, $\omega = 5.791$ THz (d) Field profile of $|E_x|$, $|E_y|$ for upper mode with values $\beta = 0.266\ \mu\text{m}^{-1}$, $\omega = 6.537$ THz.

4. Concluding remarks

The surface optics approach was utilized to study the characteristics of polaritonic interactions at the chiral–TSM interface. In the presence of the chiral material, the splitting of the phononic and plasmonic modes was reported, and the existence of trends similar to those seen in the chiral material-based microcavity system was identified. Here, the hybrid modes of propagation were labeled as the lower and upper modes. The field profiles revealed that the upper modes corresponded to the surface evanescent polariton modes, while the lower modes corresponded to the chiral polaritons non-degenerate modes. It was found that the propagation gap between the lower and upper modes could be tuned or detuned by the CD or chiral strength of the chiral material. Further, the resonance frequency and type of polaritonic (phononic/plasmonic) interaction could be controlled by the external temperature of the TSM. The results may have significant importance in thermo-chiral and optical sensing, enantiomeric detection, and near-field communications.

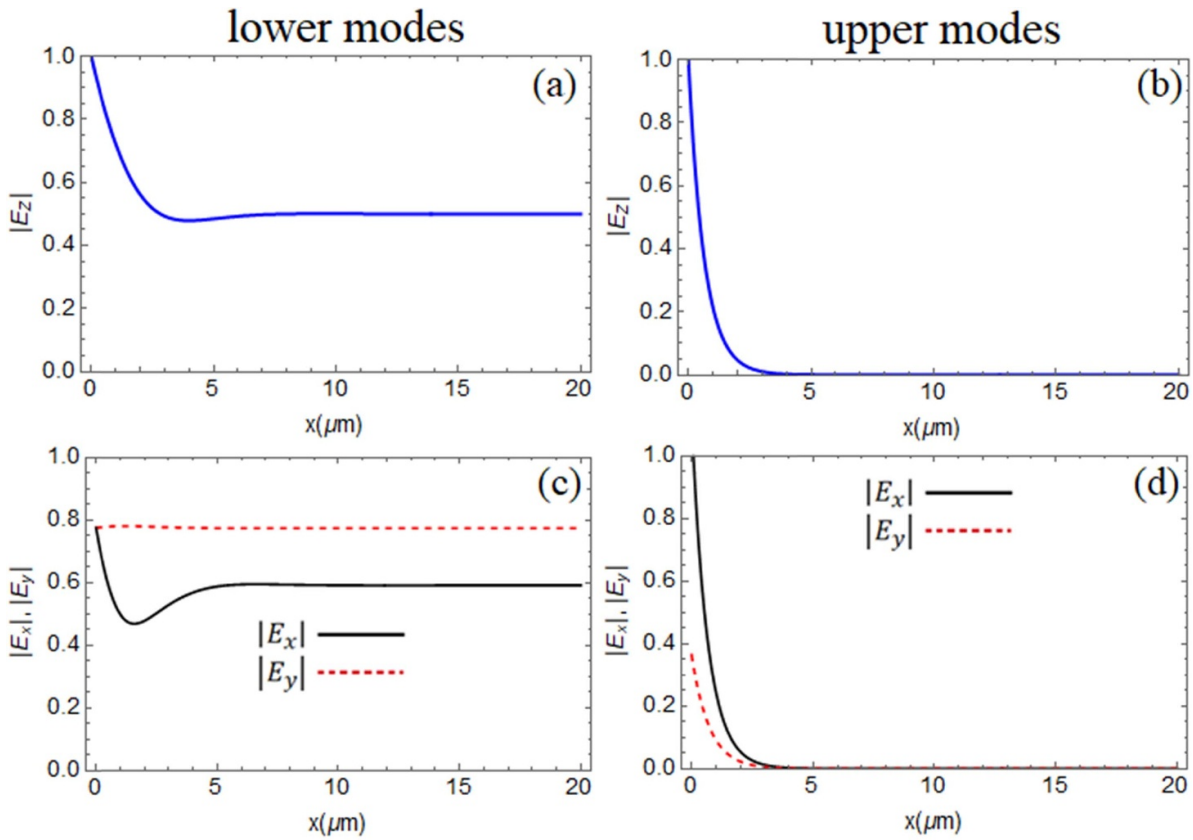

Figure 11. Field distribution as function of transverse distance at chiral–InSb interface $T = 300$ K (metallic state), with $\xi = 0.01\Omega^{-1}$ & $\varepsilon_c = 2.25\ \varepsilon_o$ (a) Field profile of $|E_z|$ for lower mode with values $\beta = 0.0825\ \mu\text{m}^{-1}$, $\omega = 5.791$ THz, (b) Field profile of $|E_z|$ for upper mode with values $\beta = 0.266\ \mu\text{m}^{-1}$, $\omega = 6.537$ THz, (c) Field profile of $|E_x|$, $|E_y|$ for lower mode with values $\beta = 0.0825\ \mu\text{m}^{-1}$, $\omega = 5.791$ THz, (d) Field profile of $|E_x|$, $|E_y|$ for upper mode with values $\beta = 0.266\ \mu\text{m}^{-1}$, $\omega = 6.537$ THz.

Data availability statement

All data that support the findings of this study are included within the article (and any supplementary files).

Availability of Data and Materials

Detail about data has been provided in the article.

Acknowledgments

This work was supported by the Researchers Supporting Project number.

(RSPD2025R985), King Saud University, Riyadh, Saudi Arabia.

Conflict of interest

The authors declare that they have no known competing financial interests or personal relationships that could have appeared to influence the work reported in this paper.

ORCID iDs

Ahtisham Ali https://orcid.org/0009-0008-8052-1346
Muhammad Zeshan Yaqoob https://orcid.org/0000-0001-9145-8604
Majeed A S Alkanhal https://orcid.org/0000-0003-3673-0411

References

[1] Luo T, Ilyas B, Hoegen A V, Lee Y, Park J, Park J-G and Gedik N 2024 Time-of-flight detection of terahertz phonon-polariton *Nat. Commun.* **15** 1–8
[2] Rajabali S, Cortese E, Beck M, De Liberato S, Faist J and Scalari G J N P 2021 Polaritonic nonlocality in light–matter interaction *Nat. Photon.* **15** 690–5
[3] Basov D N, Asenjo-Garcia A, Schuck P J, Zhu X and Rubio A J N 2020 Polariton panorama *Nanophotonics* **10** 549–77
[4] Zhang F, Pei J, Baev A, Samoc M, Ge Y, Prasad P N and Zhang H J P R 2022 Photo-dynamics in 2D materials: processes, tunability and device applications *Phys. Rep.* **993** 1–70
[5] Mandal A, Taylor M A, Weight B M, Koessler E R, Li X and Huo P J C R 2023 Theoretical advances in polariton chemistry and molecular cavity quantum electrodynamics *Chem. Rev.* **123** 9786–879
[6] Agranovich V M 2012 *Surface Polaritons* (Elsevier)

[7] Sanvitto D and Kéna-Cohen S J N M 2016 The road towards polaritonic devices *Nat. Mater.* **15** 1061–73

[8] Meng F, Cao L, Mangeney J and Roskos H G J N 2024 Strong coupling of metamaterials with cavity photons: toward non-Hermitian optics *Nanophotonics* **13** 2443–51

[9] Abdullah S, Dias E J, Krpensky´J, Mkhitaryan V and García de Abajo F J J A P 2024 Toward complete optical coupling to confined surface polaritons *ACS Photonics* **11** 2183–93

[10] Santos P and Fainstein A J O M E 2023 Polaromechanics: polaritonics meets optomechanics *Opt. Mater. Express* **13** 1974–83

[11] Harrison S L, Nalitov A, Lagoudakis P G and Sigurðsson H J O M E 2023 Polariton vortex Chern insulator *Opt. Mater. Express* **13** 2550–62

[12] Baranov D G, Munkhbat B, Länk N O, Verre R, Käll M and Shegai T J N 2020 Circular dichroism mode splitting and bounds to its enhancement with cavity-plasmon-polaritons *Nanophotonics* **9** 283–93

[13] Bennenhei C, Struve M, Stephan S, Kunte N, Mitryakhin V N, Eilenberger F, Ohmer J, Fischer U, Silies M and Schneider C J O M E 2023 Polarized room-temperature polariton lasing in elliptical microcavities filled with fluorescent proteins *Opt. Mater. Express* **13** 2633–43

[14] Król M, Łempicka-Mirek K, Rechcińska K, Furman M, Nogajewski K, Mazur R, Morawiak P, Piecek W, Pacuski W and Szczytko J J O M E 2023 Universality of open microcavities for strong light-matter coupling *Opt. Mater. Express* **13** 2651–61

[15] Salij A H, Goldsmith R H and Tempelaar R J N C 2024 Theory predicts 2D chiral polaritons based on achiral Fabry–Pérot cavities using apparent circular dichroism *Nat. Commun.* **15** 340

[16] Mohammadi Estakhri N, Edwards B and Engheta N J S 2019 Inverse-designed metastructures that solve equations *Science* **363** 1333–8

[17] La Spada L and Vegni L J O E 2017 Near-zero-index wires *Opt. Express* **25** 23699–708

[18] Lalegani Z, Ebrahimi S S, Hamawandi B, La Spada L, Batili H and Toprak M J M C 2022 Targeted dielectric coating of silver nanoparticles with silica to manipulate optical properties for metasurface applications *Mater. Chem. Phys.* **287** 126250

[19] Heydari M B and Samiei M H V 2018 Plasmonic graphene waveguides: a literature review (arXiv:1809.09937)

[20] Anker J N, Hall W P, Lyandres O, Shah N C, Zhao J and Van Duyne R P 2008 Biosensing with plasmonic nanosensors *Nat. Mater.* **7** 442–53

[21] Greybush N J, Pacheco-Peña V, Engheta N, Murray C B and Kagan C R J A N 2019 Plasmonic optical and chiroptical response of self-assembled Au nanorod equilateral trimers *ACS Nano* **13** 1617–24

[22] Wu T, Kessler J and Bouř P 2016 Chiral sensing of amino acids and proteins chelating with Eu III complexes by Raman optical activity spectroscopy *Phys. Chem. Chem. Phys.* **18** 23803–11

[23] Berova N, Polavarapu P L, Nakanishi K and Woody R W 2012 *Comprehensive Chiroptical Spectroscopy, Volume 2: Applications in Stereochemical Analysis of Synthetic Compounds, Natural Products, and Biomolecules* 2 (Wiley)

[24] Hentschel M, Schäferling M, Duan X, Giessen H and Liu N 2017 Chiral plasmonics *Sci. Adv.* **3** e1602735

[25] Mi G and Van V 2014 Characteristics of surface plasmon polaritons at a chiral–metal interface *Opt. Lett.* **39** 2028–31

[26] Nag A, Simorangkir R B, Gawade D R, Nuthalapati S, Buckley J L, O'Flynn B, Altinsoy M E and Mukhopadhyay S C J M 2022 Graphene-based wearable temperature sensors: a review *Mater. Des.* **221** 110971

[27] Kang M, Jeong H, Park S-W, Hong J, Lee H, Chae Y, Yang S and Ahn J-H J S A 2022 Wireless graphene-based thermal patch for obtaining temperature distribution and performing thermography *Sci. Adv.* **8** eabm6693

[28] Chen S, Jiang K, Lou Z, Chen D and Shen G J A M T 2018 Recent developments in graphene-based tactile sensors and E-skins *Adv. Mater. Technol.* **3** 1700248

[29] Yaqoob M, Ghaffar A, Alkanhal M, Rehman S U and Razzaz F J S R 2018 Hybrid surface plasmon polariton wave generation and modulation by chiral-graphene-metal (CGM) structure *Sci. Rep.* **8** 18029

[30] Yaqoob M, Ali A, Alkanhal M A, Ghaffar A, Khan Y and Umair M 2024 Temperature-dependent electromagnetic surface wave supported by graphene-loaded indium antimonide planar structure *Int. J. Opt.* **2024** 9607121

[31] Wuttig M, Bhaskaran H and Taubner T J N P 2017 Phase-change materials for non-volatile photonic applications *Nat. Photon.* **11** 465–76

[32] Liu H, Ren G, Gao Y, Lian Y, Qi Y and Jian S 2015 Tunable subwavelength terahertz plasmon-induced transparency in the InSb slot waveguide side-coupled with two stub resonators *Appl. Opt.* **54** 3918–24

[33] Yaqoob M, Ahamd M, Ghaffar A, Razzaz F, Saeed S and Alanazi T J S R 2023 Thermally tunable electromagnetic surface waves supported by graphene loaded indium antimonide (InSb) interface *Sci. Rep.* **13** 18631

[34] Schäferling M J S S I O S 2017 *Chiral nanophotonics* 205 p 159 (Springer)

[35] Baranov D G, Schäfer C and Gorkunov M V J A P 2023 Toward molecular chiral polaritons *ACS Photonics* **10** 2440–55

[36] Yaqoob M Z, Ghaffar A, Alkanhal M and Rehman S U J J O T O S O A B 2018 Characteristics of light–plasmon coupling on chiral–graphene interface *J. Opt. Soc. Am.* B **36** 90–95

[37] Moradi M J S R 2023 Thermally tunable Dyakonov surface waves in semiconductor nanowire metamaterials *Sci. Rep.* **13** 12353

[38] Anderson W E, Alexander R W Jr and Bell R J J P R L 1971 Surface plasmons and the reflectivity of n-type InSb *Phys. Rev. Lett.* **27** 1057

[39] Maier S A 2007 *Plasmonics: Fundamentals and Applications* (Springer)

[40] Mackay T G and Lakhtakia A 2016 Simultaneous amplification and attenuation in isotropic chiral materials *J. Opt.* **18** 055104